EUROGRAPHICS 2007 / D. Cohen-Or and P. Slavík
(Guest Editors)

Volume 26 (2007), Number 3

Skeleton-based Variational Mesh Deformations

Shin Yoshizawa [1] Alexander Belyaev [2] Hans-Peter Seidel [2]

[1] RIKEN [2] MPI Informatik

Abstract

In this paper, a new free-form shape deformation approach is proposed. We combine a skeleton-based mesh deformation technique with discrete differential coordinates in order to create natural-looking global shape deformations. Given a triangle mesh, we first extract a skeletal mesh, a two-sided Voronoi-based approximation of the medial axis. Next the skeletal mesh is modified by free-form deformations. Then a desired global shape deformation is obtained by reconstructing the shape corresponding to the deformed skeletal mesh. The reconstruction is based on using discrete differential coordinates. Our method preserves fine geometric details and original shape thickness because of using discrete differential coordinates and skeleton-based deformations. We also develop a new mesh evolution technique which allow us to eliminate possible global and local self-intersections of the deformed mesh while preserving fine geometric details. Finally, we present a multi-resolution version of our approach in order to simplify and accelerate the deformation process. In addition, interesting links between the proposed free-form shape deformation technique and classical and modern results in the differential geometry of sphere congruences are established and discussed.

Categories and Subject Descriptors (according to ACM CCS): I.3.5 [Computer Graphics]: Computational Geometry and Object Modeling

1. Introduction

Global free-form mesh deformations is an active research area which is greatly stimulated by demands of the digital entertainment industry. Each year brings new approaches as well as combinations and reworking of old favorites [BSPG06, BPGK06, FTS06, HSL*06, JSW05, LSCOL05]. and this year is not an exception [BPWG07, LCOGL07, JMD*07, KMP07] In particular, skeleton-based mesh deformation techniques remain powerful and competitive [YBS03, DQ04, LKA06, YHM06, IBP07, WSLG07].

In this paper, we propose a new approach to skeleton-based global mesh deformations. Conceptually our approach to free-form shape deformations is quite simple. Given a 3D solid, we extract its Blum skeleton and represent the boundary of the solid as the envelope of spheres whose centers lie on the skeleton. The boundary is now determined by the geometry of the skeleton and a radial vector field from the sphere centers to the boundary of the solid. (Each sphere centered at a regular point of the skeleton has two points of tangency with the envelope and, therefore, defines two radial vectors from the sphere center to the tangency points. In order to define properly the radial vector field we distinguish two sides of the skeleton: each regular skeleton point is duplicated and each duplicate is assigned with its corresponding radial vector.) A free-form deformation is then applied to the skeleton while the radial vectors and their relative positions (w.r.t. the skeleton) are preserved. The deformed shape is now reconstructed for the deformed skeleton and its radial vector field. Mathematical aspects of such surface reconstruction and representation is currently a subject of intensive research [GK03, Dam05, Dam07].

The idea of skeleton-based shape deformations was proposed by Blum, the inventor of the skeleton [Blu67]. (The Blum skeleton is also known under the name of Medial Axis, but we prefer to call it "skeleton" since for generic 3D shapes it consists of a set of surface patches glued together.) In his seminal paper [Blu73], Blum suggested to consider the so-called *flexures*, shape deformations which changes the skeleton of a plane figure while maintaining the object's width associated with the skeleton. In graphics and modeling, skeleton-based deformation techniques [BL99, Blo02, YBS03] appeared as natural generalizations of metaballs [Bli82] and convolution surfaces [BS91]. At

© The Eurographics Association and Blackwell Publishing 2007. Published by Blackwell Publishing, 9600 Garsington Road, Oxford OX4 2DQ, UK and 350 Main Street, Malden, MA 02148, USA.

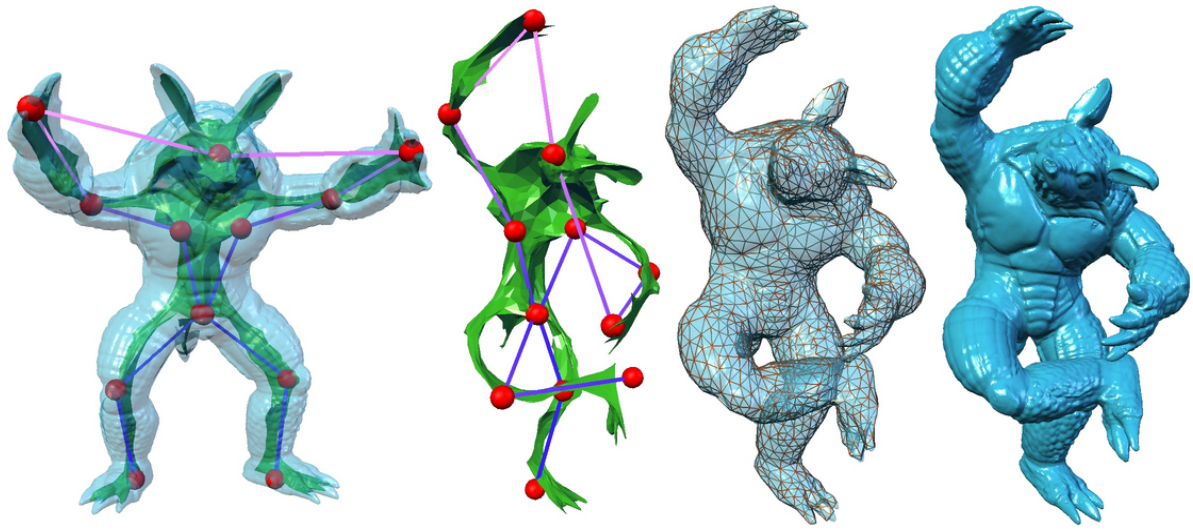

(a) (b) (c) (d)

Figure 1: *A skeleton-based variational mesh deformation example. (a): The Armadillo model represented according to the Displaced Subdivision Surface (DSS) multi-resolution scheme [LMH00] (332K triangles), the skeletal mesh computed for the DSS base mesh (5K triangles), and a stick-figure skeleton to be used for a deformation of the skeleton. (b): A Skeletal Subspace Deformation (SSD) [MTLT88, LCJ94] is applied to the skeletal mesh. (c): A deformation of the DSS control mesh is obtained by using discrete differential coordinates associated with the deformed skeletal mesh. (d): Displacement details are added to the deformed DSS control mesh.*

present skeleton-based shape manipulations are widely used for biomedical image analysis purposes [PFF*03].

Surprisingly shape deformations similar to Blum's flexures were considered fifty years earlier by Bianchi [Bia23, Chap. XIX] in connection with his study of families of spheres (sphere congruences) and their envelopes. One remarkable Bianchi's result is that *given a two-parameter family of spheres and its envelope, if the locus of the centers is bended the two points of contact of each sphere with the envelope retain invariable positions*. (A simple proof of this statement is given in Appendix A of our paper.) This observation is at the heart of our approach.

Of course, a practical realization of the above general theoretical strategy for skeleton-based deformations is far from being simple. First of all, a robust extraction of the skeleton and the radial field is a difficult problem. Second, shape reconstruction from the deformed skeleton and the corresponding radial vector field is a tough computational task. Next, the reconstructed shape may have (and usually has) self-intersections and further post-processing procedures are needed to eliminate them. Finally, straightforward implementing of the above approach for complex shapes approximated by large-size meshes is time consuming and, therefore, not practical.

In our approach, we combine a skeleton-based mesh deformation technique with discrete differential coordinates [Ale03, Sor06] in order to create natural-looking global shape deformations. Given a triangle mesh, we first extract a skeletal mesh, a two-sided Voronoi-based approximation of the skeleton (medial axis). Next the skeletal mesh is modified by free-form deformations. Then a desired global shape deformation is obtained by reconstructing the shape corresponding to the deformed skeletal mesh. The reconstruction is based on using discrete differential coordinates. Our method preserves fine geometric details and original shape thickness because of using discrete differential coordinates and skeleton-based deformations. We also develop a new mesh evolution technique which allow us to eliminate possible global and local self-intersections of the deformed mesh while preserving fine geometric details. Finally, we present a multi-resolution version of our approach in order to simplify and accelerate the deformation process. The main stages of our approach are demonstrated in Fig. 1 and typical mesh deformations are also shown in Fig. 2.

2. Skeleton extraction and deforming

Consider a closed surface $\mathcal{M}$ and its skeletal structure $(\mathcal{S}, R)$, where $\mathcal{S}$ is the skeleton of $\mathcal{M}$ and R is the corresponding radial function. Following [HBK02, YBS03, Dam05, Dam07] let us consider the "double" of $\mathcal{S}$, the surface generated by stretching $\mathcal{M}$ over $\mathcal{S}$ by the so-called grassfire flow moving $\mathcal{M}$ in the direction of its inward normal with unit speed (see, for example, [Dam05] for a mathe-

© The Eurographics Association and Blackwell Publishing 2007.

Figure 2: *Gymnastic exercises for Armadillo.*

matically rigorous definition of the double skeleton and nice illustrations). Topologically the double skeleton $\tilde{\mathcal{S}}$ is an ordinary two-sided surface homotopically equivalent to $\mathcal{M}$. Geometrically $\tilde{\mathcal{S}}$ is not, in general, a smooth surface: it has sharp edges at the singularities of the skeleton $\mathcal{S}$. The one-to-one correspondence between the points of $\mathcal{M}$ and $\tilde{\mathcal{S}}$ can be represented by the equation

$$\mathcal{M} = \tilde{\mathcal{S}} + RN, \tag{1}$$

where N denotes the field of outer normal of $\mathcal{M}$. In the rest of this paper, we simplify notations by denoting the double skeleton $\tilde{\mathcal{S}}$ by $\mathcal{S}$.

In geometric modeling, shape representation (1) was introduced in [SPW96].

Now we consider a discrete setting and assume that $\mathcal{M}$ is a triangle mesh. The corresponding skeletal mesh $\mathcal{S}$ is generated as follows. First the Quickhull algorithm [BDH96] is used to compute the Voronoi diagram of the set of vertices of $\mathcal{M}$ and for each vertex its Voronoi cell is determined. Then the vertices of $\mathcal{S}$ are computed as the inner Voronoi poles [ABK98]. Finally the connectivity (topology) of $\mathcal{S}$ is inherited from the connectivity of $\mathcal{M}$. The resulting skeletal mesh $\mathcal{S}$ satisfies (1) where N is the set of the corresponding outer mesh normals at the vertices of $\mathcal{M}$.

It is well known that the skeleton of a shape is highly sensitive to even small perturbations of the shape. However we are not interested in a very accurate extraction of the skeleton since inaccuracies can be compensated by the radial function R in (1). We gently simplify the geometry of the skeleton by applying a variant of the bi-Laplacian tangential flow [WSGD00] to the skeletal mesh. Namely, the bi-Laplacian tangential flow is applied only to those vertices

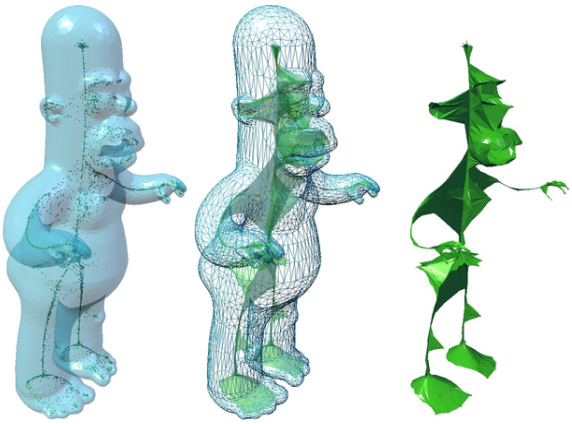

Figure 3: *Skeletal mesh extraction. Left: Homer mesh and its Voronoi poles. Center: the triangulation of the Voronoi poles inherits the Homer mesh connectivity. Right: the resulting skeletal mesh.*

of $\mathcal{S}$ for which the inner product between the flow speed vector and the displacement vector in (1) is negative. The flow mostly acts on the skeleton's sharp edges where the density of the skeletal mesh vertices is high and the angle between the flow speed and $\mathbf{n}$, the outer normal of $\mathcal{M}$, is obtuse. Thus the flow reduces geometric complexity of the skeleton. Finally, the radial function R is appropriately updated.

Any intuitive free-form deformation technique for the skeletal mesh seems appropriate for our approach. In particular, inspired by [MTLT88, LCJ94, Blo02] we implemented a Skeletal Subspace Deformation (SSD) scheme. The de-

© The Eurographics Association and Blackwell Publishing 2007.

formations of the skeletal mesh are controlled by deformations of a stick-figure skeleton built manually for the skeletal mesh, as seen in Fig. 1.

3. Mesh reconstruction from deformed skeleton

Our task now is to reconstruct a deformed mesh $\mathcal{M}_d$ using the deformed skeletal mesh $\mathcal{S}_d$ and radial field R.

First, a fragmented mesh $\mathcal{M}_F$ (a triangle soup) is generated by applying local transformations to all triangles of $\mathcal{M}$ where the transformations are defined by according to the local frames attached $\mathcal{S}$ and $\mathcal{S}_d$. Then $\mathcal{M}_d$ is obtained by stitching the fragmented mesh triangles based on minimizing and redistributing a deformation error. Here the error is given by a squared difference between the discrete differential coordinates of $\mathcal{M}_F$ and $\mathcal{M}_d$. Similar strategies were applied for stitching fragmented meshes in [SP04, YZX*04, ZRKS05].

Let $\mathbf{x}$, $\mathbf{s}$, and $\mathbf{s}^d$ be the corresponding vertices of meshes $\mathcal{M}$, $\mathcal{S}$, and $\mathcal{S}_d$, respectively. According to (1) the corresponding vertex of the deformed mesh $\mathcal{M}_d$ should computed by

$$\mathbf{x}^d = \mathbf{s}^d + R\,\mathbf{n}^d, \tag{2}$$

where $R = |\mathbf{x}-\mathbf{s}|$ is the radius of the medial ball of $\mathcal{M}$ centered at $\mathbf{s}$, as seen in Fig. 4. In practice, instead of (2) a similar shift transformation is applied to the triangles of the deformed skeletal mesh $\mathcal{S}_d$.

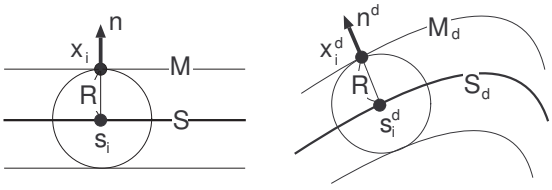

Figure 4: *Left: a given shape is represented as an envelope of spheres centered at the skeleton of the shape. Deforming the skeleton while preserving the sphere radii implies a global shape deformation.*

Let $\{\mathbf{x}_i,\mathbf{x}_j,\mathbf{x}_k\}$, $\{\mathbf{s}_i,\mathbf{s}_j,\mathbf{s}_k\}$, and $\{\mathbf{s}_i^d,\mathbf{s}_j^d,\mathbf{s}_k^d\}$ be corresponding triangles of $\mathcal{M}$, $\mathcal{S}$, and $\mathcal{S}_d$, respectively. Denote by $\mathbf{B}_0 = \left(\mathbf{v}_0,\mathbf{t}_0^1,\mathbf{t}_0^2\right)$ a basis-vector frame defined by the skeletal mesh triangle $\{\mathbf{s}_i,\mathbf{s}_j,\mathbf{s}_k\}$. Here

$$\mathbf{t}_0^1 = \frac{\mathbf{s}_j-\mathbf{s}_i}{|\mathbf{s}_j-\mathbf{s}_i|}, \quad \mathbf{t}_0^2 = \frac{\mathbf{s}_k-\mathbf{s}_i}{|\mathbf{s}_k-\mathbf{s}_i|}, \quad \text{and} \quad \mathbf{v}_0 = \mathbf{t}_0^1 \times \mathbf{t}_0^2.$$

The corresponding basis-vector frame for $\{\mathbf{s}_i^d,\mathbf{s}_j^d,\mathbf{s}_k^d\}$ is computed similarly. See Fig. 5 for an illustration.

It is accurate and computationally robust to approximate the normal $\mathbf{n}_i$ of $\mathcal{M}$ at $\mathbf{x}_i$ by $(\mathbf{x}_i-\mathbf{s}_i)/|\mathbf{x}_i-\mathbf{s}_i|$ [DS06]. Now

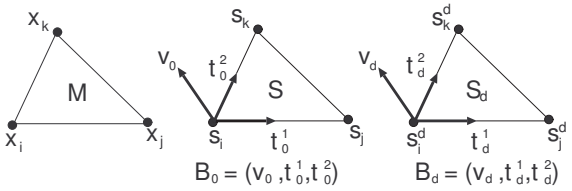

Figure 5: *Corresponding triangles of $\mathcal{M}$, $\mathcal{S}$, and $\mathcal{S}_d$. Local coordinate frames are attached to the corresponding triangles of $\mathcal{S}$ and $\mathcal{S}_d$.*

the local coordinate transform $\mathbf{B}_d\mathbf{B}_0^{-1}$ defined for each triangle T of $\mathcal{S}_d$ is used to approximate $\mathbf{n}_i^d$:

$$\mathbf{n}_i^d = \mathbf{B}_d\mathbf{B}_0^{-1}(\mathbf{x}_i-\mathbf{s}_i)\Big/\left|\mathbf{B}_d\mathbf{B}_0^{-1}(\mathbf{x}_i-\mathbf{s}_i)\right|.$$

The vertices of fragmented mesh $\mathcal{M}_F$ are given by

$$\mathbf{x}_i^F = \mathbf{s}_i^d + R_i\mathbf{n}_i^d. \tag{3}$$

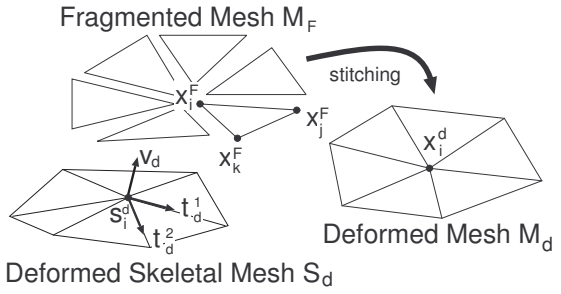

Figure 6: *Skeleton-based variational mesh deformation framework. First fragmented mesh (triangle soup) $\mathcal{M}_F$ is generated from deformed skeletal mesh $\mathcal{S}_d$. Then differential coordinates are used for stitching the triangles of $\mathcal{M}_F$.*

Our task now is to reconstruct a deformed mesh $\mathcal{M}_d$ from fragmented mesh $\mathcal{M}_F$, as seen in Fig. 6. One possible solution [KO03] consists of generating vertex positions $\mathbf{x}_i^d \in \mathcal{M}_d$ via simple averaging the positions of the corresponding vertices of the the fragmented mesh $\mathcal{M}_F$. While this approach seems attractive because of its simplicity, better reconstruction results are usually achieved when differential mesh coordinates are employed for the reconstruction [YZX*04, ZRKS05, ZHS*05]. Further, the use of differential coordinates allows us to easily take into account the influence of the deformed skeletal mesh $\mathcal{S}_d$.

Consider the graphs $\mathcal{G}$ and $\mathcal{G}_F$ composed from the pairs of meshes $\{\mathcal{M},\mathcal{S}\}$ and $\{\mathcal{M}_F,\mathcal{S}_d\}$, respectively. The connectivity structures of $\mathcal{G}$ and $\mathcal{G}_F$ are shown in Fig. 7.

Let us equip the edges of $\mathcal{G}$ and $\mathcal{G}_F$ with weights. Each

© The Eurographics Association and Blackwell Publishing 2007.

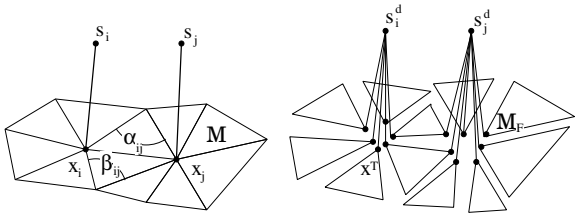

Figure 7: *Graphs $\mathcal{G}$ (left) and $\mathcal{G}_F$ (right).*

edge $(\mathbf{x}_i,\mathbf{x}_j)$ of $\mathcal{G}$ is assigned with the standard cotan weight $w(\mathbf{x}_i,\mathbf{x}_j)=\cot\alpha_{ij}+\cot\beta_{ij}$ [PP99] where α_{ij} and β_{ij} are the angles opposite to $(\mathbf{x}_i,\mathbf{x}_j)$ in $\mathcal{M}$, as seen in the left image of Fig. 7. The edges connecting $(\mathbf{x}_i,\mathbf{s}_i)$ are assigned with the unit weights $w(\mathbf{x}_i,\mathbf{s}_i)=1$. For a triangle $(\mathbf{x}_i^F\mathbf{x}_k^F\mathbf{x}_j^F)$ of $\mathcal{G}_F$, the triangle edge $(\mathbf{x}_i^F,\mathbf{x}_j^F)$ is equipped with the weight $w_f(\mathbf{x}_i^F,\mathbf{x}_j^F)=\cot\angle\mathbf{x}_i\mathbf{x}_k\mathbf{x}_j$ where the angle is measured in $\mathcal{M}$. The edges connecting $(\mathbf{x}_i^F,\mathbf{s}_i^d)$ are assigned with weights $w(\mathbf{x}_i^F,\mathbf{s}_i^d)=1/N_i$, where N_i is the number of the one-link neighborhood triangles of $\mathbf{x}_i$ in $\mathcal{M}$.

Once $\mathcal{G}$ and $\mathcal{G}_F$ become weighted graphs, the graph-Laplacians of $\mathcal{G}$ and $\mathcal{G}_F$ are appropriately defined [Chu97]. Let $\mathbf{L}$ be the Laplacian matrix of $\mathcal{M}$. Then the list of vertices $\mathbf{x}^d=\{\mathbf{x}_i^d\}$ of the deformed mesh $\mathcal{M}_d$ is determined from $\mathbf{x}^F=\{\mathbf{x}_i^F\}$ and $\mathbf{s}^d=\{\mathbf{s}_i^d\}$ by solving

$$\boldsymbol{L}\begin{bmatrix}\mathbf{x}^d\\ \mathbf{s}^d\end{bmatrix}\equiv\begin{pmatrix}\mathbf{I}+\mathbf{L} & -\mathbf{I}\\ \mathbf{0} & \mathbf{I}\end{pmatrix}\begin{bmatrix}\mathbf{x}^d\\ \mathbf{s}^d\end{bmatrix}=\begin{bmatrix}\mathbf{y}\\ \mathbf{s}^d\end{bmatrix},\quad(4)$$

where the list of vertices $\mathbf{y}=\{\mathbf{y}_i\}$ is generated from the vertices of $\mathcal{G}_F$ by

$$\mathbf{y}_i=\sum_{(j,k)}w_1(\mathbf{x}_i^F-\mathbf{x}_j^F)+w_2(\mathbf{x}_i^F-\mathbf{x}_k^F)+\frac{\mathbf{x}_i^F-\mathbf{s}_i^d}{N_i}.$$

Here the sum is taken over the set of index pairs (j,k) corresponding to the edges of $\mathcal{M}$ opposite to vertex $\mathbf{x}_i\in\mathcal{M}$, $w_1=\cot\angle\mathbf{x}_i\mathbf{x}_k\mathbf{x}_j$, $w_2=\cot\angle\mathbf{x}_i\mathbf{x}_j\mathbf{x}_k$.

Notice that $\mathbf{y}$ can be considered as the result of applying the graph-Laplacian of $\mathcal{G}_F$ to the vertices of $\mathcal{M}_F$.

One can easily see that the vertices $\mathbf{x}^d$ obtained from (4) depend only on $\mathbf{x}^F$, the vertices of the fragmented $\mathcal{M}_F$, and can be determined by solving a simpler sparse linear system

$$(\mathbf{I}+\mathbf{L})\,\mathbf{x}^d=\tilde{\mathbf{y}},\quad\tilde{\mathbf{y}}_i=\sum w_1(\mathbf{x}_i^F-\mathbf{x}_j^F)+w_2(\mathbf{x}_i^F-\mathbf{x}_k^F)+\frac{\mathbf{x}_i^F}{N_i}.\quad(5)$$

However, as we will see later, the operator $\boldsymbol{L}$ in (4) turns out to be very useful for removing possible self-intersections of $\mathcal{M}_d$.

Multi-resolution representation. In order to process large-size models and accelerate our mesh deformation technique we have implemented a Displaced Subdivision Surface (DSS) approach of [LMH00] (without its computationally expensive optimization stage). The skeletal mesh is extracted from the coarse DSS control mesh. Then the control mesh is deformed as described above. Finally, fine shape features are reconstructed by subdividing the deformed control mesh and adding displacements along the normals of the subdivided deformed mesh.

In Fig. 8, we demonstrate advantages of using DSS. In addition to a great acceleration of the deformation process, the DSS control mesh has a much simple skeleton which provides the user with a better control for global shape deformations.

Dense mesh and its corresponding skeletal mesh

DSS control mesh and its skeletal mesh (5.2K triangles)

	Number of Triangles	Editing Skeleton	Updating Geometry	DSS	Total
	346K	94 s	1023 s		1117 s
DSS	5.2+332K	**0.13 s**	**0.3 s**	3.8 s	**4.23 s**

Figure 8: *Adding a multi-resolution mesh representation (we use a simplified version of DSS of [LMH00]) greatly accelerates the deformation process and simplifies the user control. The table presents timing measurements corresponding to the mesh deformation shown in Fig. 1.*

4. Removing mesh self-intersections

The deformed mesh $\mathcal{M}_d$ approximates the envelope of spheres centered at $\mathcal{S}_d$ and may contain self-intersections, as seen in the left image of Fig. 9. A natural way to avoid such self-intersections is to consider the boundary of the boolean union of the balls bounded by the spheres, as seen in the

© The Eurographics Association and Blackwell Publishing 2007.

right image of Fig. 9. The boolean union can be described by a function

$$f(\mathbf{z}) = \min_i \left\{ \mathbf{z} \in \mathbb{R}^3 : |\mathbf{z} - \mathbf{s}_i^d| - R_i, \quad \mathbf{s}_i^d \in \mathcal{S}_d \right\} \qquad (6)$$

and the boundary of the union is given by the equation

$$f(\mathbf{z}) = 0. \qquad (7)$$

Therefore it seems natural to resolve self-intersections of $\mathcal{M}_d$ by moving its vertices towards (7).

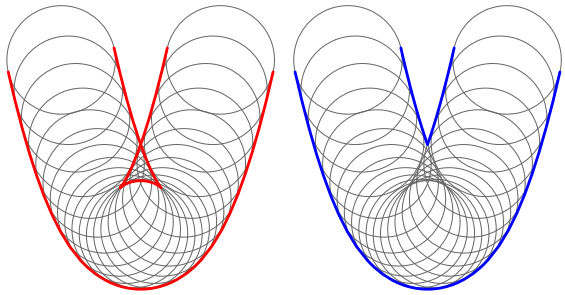

Figure 9: *Envelope vs. Union. Left: the envelope of a family of spheres. Right: the boundary of the union of the corresponding balls.*

Consider the graph $\mathcal{G}(t)$ composed from the vertices $\mathbf{x} = \{\mathbf{x}_i\}$ and $\mathbf{s}^d = \{\mathbf{s}_i^d\}$ of moving mesh $\mathcal{M}(t)$ and the deformed skeleton $\mathcal{S}_d$, respectively. In order to move $\mathcal{M}(t)$ towards (7) we use the antigradient of $\frac{1}{2}f^2$ and evolve the graph by

$$\frac{\partial[\boldsymbol{L}\mathcal{G}(t)]}{\partial t} = F(\mathcal{G}(t)) \equiv \begin{cases} -f(\mathbf{z})\nabla f(\mathbf{z}) & \text{if} \quad \mathbf{z} = \mathbf{x}^d \\ 0 & \text{if} \quad \mathbf{z} = \mathbf{s}^d \end{cases} \qquad (8)$$

where the evolution starts from the deformed mesh and its skeleton $\mathcal{G}(0) = (\mathcal{M}_d, \mathcal{S}_d)$ and $\boldsymbol{L}$ is defined in (5) and remains constant during (8). Note that the skeletal mesh $\mathcal{S}_d$ is also not affected by (8) but serves as an anchor for $\mathcal{M}(t)$.

To solve (8) numerically we consider the following semi-implicit scheme

$$\mathbf{u}^{n+1} = \mathbf{u}^n + \tau \boldsymbol{L}^{-1} F(\mathbf{u}^n), \qquad (9)$$

where $\mathbf{u}^0 = (\mathbf{x}^d, \mathbf{s}^d)$ and τ is a step-size parameter. The matrix $\boldsymbol{L}^{-1}$ is already computed† when (4) was solved and remains the same during the above graph evolution (9).

Resolving mesh self-intersections by applying an appropriately defined mesh evolution was previously used in [YBS03]. Our mesh evolution scheme (9) is simpler than that employed in [YBS03]. In addition, (9) treats the vertices of the skeletal mesh $\mathcal{S}_d$ as anchors and prevents developing defects similar to that shown in the left image of Fig. 10.

† Sparse direct solver [Dav04] is employed to compute $\boldsymbol{L}^{-1}$.

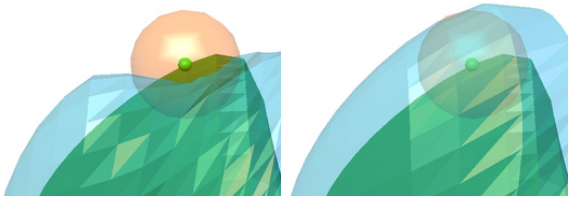

Figure 10: *Preconditioning with $\boldsymbol{L}^{-1}$ in (9) allows us to avoid defects similar to that shown in the left image. Such defects appear because of a discrete nature of our approximation to the envelope of spheres. Skeletal mesh $\mathcal{S}_d$ serves as an anchor in (9) and a correct approximation of the envelope is achieved, as seen in the right image.*

The power of our approach to resolve mesh self-intersections is demonstrated in Fig. 11. Note that mesh evolution (9) improves the accuracy of the deformed mesh by pushing it towards the boundary of the union of the medial balls (an example of such a union is shown in the right image of Fig. 9).

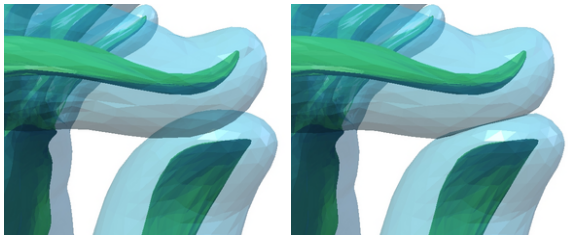

Figure 11: *Global self-intersection fairing. Left: a deformed mesh contains self-intersections. Right: evolution (9) efficiently removes the self-intersections.*

A straightforward computation of (6) and, therefore, the right-hand side of (9) is time-consuming. In order to accelerate discrete evolution (9) we simplify (6) by considering a proper subset of the medial balls centered at the vertices of $\mathcal{S}_d$.

Let us observe that for each vertex $\mathbf{u}_i = \{\mathbf{x}_i, \mathbf{s}_i^d\}$ of $\mathcal{G}(t)$ the value $f(\mathbf{x}_i)$ is bounded by $\left| |\mathbf{x}_i - \mathbf{s}_i^d| - R_i \right|$. Thus it is natural to approximate the antigradient of $\frac{1}{2}f^2$ at $\mathbf{x}_i$ by

$$-f(\mathbf{x}_i)\nabla f(\mathbf{x}_i) \approx \left(|\mathbf{x}_i - \mathbf{s}_p^d| - R_p \right) \left(\mathbf{x}_i - \mathbf{s}_p^d \right), \qquad p = \operatorname{argmin}_j \left\{ |\mathbf{x}_i - \mathbf{s}_j^d| - R_j | \right\} \qquad (10)$$

and the minimum is taken over all $\mathbf{u}_j = (\mathbf{x}_j, \mathbf{s}_j^d)$ such that $|\mathbf{x}_j - \mathbf{x}_i| \le R_i$. For fast evaluating (10) a kd-tree search structure is constructed and updated after each iteration of (9).

If a model has a complex geometry (e.g., a deformed Armadillo mesh), flow (9) is applied to the DSS control mesh of the model. For a simple model, like the ellipsoid from Fig. 9), the flow is applied to the model itself.

© The Eurographics Association and Blackwell Publishing 2007.

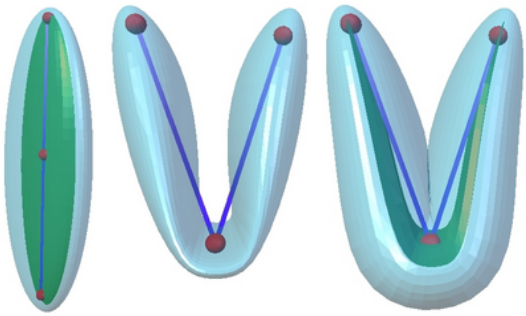

Figure 12: *A comparison of SSD [MTLT88, LCJ94] and our skeleton-based variational approaches. Left: original shape (an ellipsoid). Center: SSD is applied. Right: our method is used.*

Of course, if (9) is applied to the DSS control mesh of a model, one cannot guarantee that all intersections of the model will be removed by (9).

According to our numerical experiments, typically 10-50 iterations of (9) are needed to remove self-intersections and improve the mesh quality. Our implementation of (9) is reasonably fast. For example, it takes only 0.16s per iteration for the ellipsoid mesh from Fig. 12 (4.9K triangles) and 0.12s per iteration of the DSS control mesh of the Armadillo model. ‡

5. Discussion

The two main advantages of our mesh deformation method are preserving the thickness of the deformed models and an elegant geometric way for removing possible mesh self-intersections. To the best of our knowledge, the latter issue is very rarely addressed in the shape deformation literature. Both the advantages are natural consequences of the skeleton-based shape representation in which a given surface is represented as the envelope of spheres centered at the skeleton of the figure bounded by the surface.

In Fig. 12, we use a simple shape (an ellipsoid) to compare with the SSD technique [MTLT88, LCJ94], an axial-based shape deformation approach. In Fig. 13, the same model is used for a comparison of various techniques for shape reconstruction from a deformed skeleton.

Thickness preservation, an intrinsic property of our approach, is missed by most of the modern non-skeletal shape deformation techniques (as far as we can judge, only the rigid cell approach proposed [BPWG07] is capable to preserve thicknesses of deformed models). Several methods deliver volume-preserving deformations [ZHS*05, FTS06]. We think, however, that for many applications preserving the thicknesses of a deformed model is a desirable feature which can provide the user with a simple and intuitive control over the deformation process.

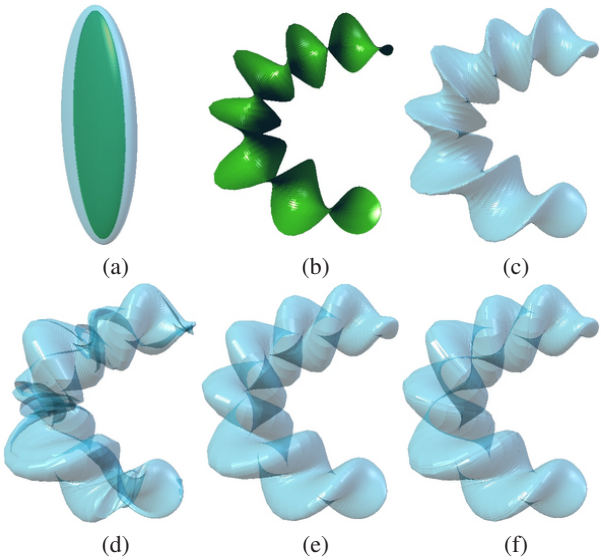

Figure 13: *A comparison of several popular schemes for computing a deformed shape from a deformed skeleton. For each deformed mesh, the computational time is given in seconds and surface approximation error ε is measured by summing up the values of (6) computed at the vertices of the deformed mesh. (a): Ellipsoid and its skeletal mesh (19.6K triangles). (b): Deformed skeletal mesh. (c): SSD method [MTLT88, LCJ94],* 2.3*s*, $\varepsilon = 20.2$. *(d): Homotopy method [YBS03] (no DSS acceleration),* 2.7*s*, $\varepsilon = 19.6$. *(e): Weighted blending [Blo02],* 14.8*s*, $\varepsilon = 11.8$. *(f): The method of this paper (no DSS acceleration)* 2.9*s*, $\varepsilon = 3.8$. *Evolution (9) decreases the approximation error:* $\varepsilon = 0.2$.

To compare with previous skeleton-based shape deformation methods, we believe that our approach provides the user with a richer set of deformations than line-skeleton techniques [LKA06, YHM06] and delivers a better preservation of shape features under larger-scale deformations than other schemes based on the classical Blum skeleton [YBS03, DQ04]. See, for example, Fig. 13 for a comparison of our approach with that developed in [YBS03].

While PriMo [BPGK06], rigid cells [BPWG07], and Volumetric Graph Laplacian [ZHS*05] techniques are capable of avoiding local self-intersections, only vector field based approaches [ACWK06, FTS06], and another skeleton-based deformation method [YBS03] are our competitors in the ability to avoid global mesh self-intersections. To compare with [YBS03] our self-intersection fairing flow (8), (9) is very fast.

Of course our method is not free from drawbacks. Some

‡ All the computations described in this paper were performed on a 1.7GHz Pentium 4 with 1GB RAM.

© The Eurographics Association and Blackwell Publishing 2007.

deformation defects can be observed on the left leg of the Homer model and the neck of the Stanford Dragon. (For the Homer model, they are especially visible because the mesh does not contain high-frequency details which usually produce a masking effect.) The problem here is that the skeleton of a canal surface degenerates into a space curve. In practice, the skeletal mesh of a model close to a canal surface is of a poor quality and certain instabilities may appear during our mesh reconstruction process.

Figure 14: *More deformation examples. Certain defects can be observed on the left leg of the Homer model and the neck of the Stanford Dragon.*

Our approach would be greatly enhanced if we were given a method for generating bending deformations (i.e., preserving the first fundamental form) of the skeletal mesh. Then, as shown in Appendix A, the first fundamental form of $\mathcal{M}$ (and, therefore, the surface area element) is also preserved in the deformation process. In addition, several global characteristics of a figure bounded by $\mathcal{M}$ are bending invariants of the skeleton $\mathcal{S}$ of the solid [Dam07, Nád68]. While producing pure bending deformations of a surface seems a difficult nonlinear problem, its approximate solution in the case of the skeleton does not look very hard. Everyone who deal with skeletons should observe that $\mathcal{S}$ in its regular points is much less curved than $\mathcal{M}$ in the corresponding points. Roughly speaking, the deformation retract $\mathcal{M} \to \mathcal{S}$ converts highly curved regions of $\mathcal{M}$ into singularities of $\mathcal{S}$. Although so far this observation is supported by rigorous mathematical statements in 2D case only (see Appendix B), results of [SSR99] suggest that the observation is mathematically valid in 3D as well.

Acknowledgements

We would like to thank the anonymous reviewers of this paper for their helpful comments and suggestions.

The models are courtesy of Stanford University (Armadillo and Dragon) and INRIA Sophia-Antpolis (Homer).

This work was supported in part by AIM@SHAPE, a Network of Excellence project (506766) within EU's Sixth Framework Programme, and Strategic Programs for R&D (President's Discretionary Fund) of RIKEN.

References

[ABK98] AMENTA N., BERN M., KAMVYSSELIS M.: A new Voronoi-based surface reconstruction algorithm. In *Proceedings of ACM SIGGRAPH* (1998), pp. 415–421.

[ACWK06] ANGELIDIS A., CANI M.-P., WYVILL G., KING S.: Swirling-sweepers: constant volume modeling. *Graphical Models (GMOD) 68*, 4 (2006). Special issue on PG'04.

[Ale03] ALEXA M.: Differential coordinates for local mesh morphing and deformation. *The Visual Computer 19*, 2-3 (2003), 105–114.

[BDH96] BARBER C. B., DOBKIN D. P., HUHDANPAA H. T.: The Quickhull algorithm for convex hulls. *ACM Transactions on Mathematical Software 22*, 4 (1996), 469–483.

[Bia23] BIANCHI L.: *Lezioni di Geometria Differenziale (Volume II, Parte prima)*. Enrico Spoerri, Pisa, 1923.

[BL99] BLOOMENTHAL J., LIM C.: Skeletal methods of shape manipulation. In *International Conference on Shape Modeling and Applications (SMI'99)* (1999), pp. 44–47.

[Bli82] BLINN J. F.: A generalization of algebraic surface drawing. *ACM Transactions on Graphics 1*, 3 (1982), 235–256.

[Blo02] BLOOMENTHAL J.: Medial-based vertex deformation. In *ACM SIGGRAPH / Eurographics Symposium on Computer Animation (SCA '02)* (2002), pp. 147–151.

[Blu67] BLUM H.: A transformation for extracting new descriptors of shape. In *Symposium on Models for the Perception of Speech and Visual Form* (1967), Wathen-Dunn W., (Ed.), MIT Press, pp. 362–380.

[Blu73] BLUM H.: Biological shape and visual science (part i). *J. of Theoretical Biology 38* (1973), 205–287.

[BPGK06] BOTSCH M., PAULY M., GROSS M., KOBBELT L.: PriMo: coupled prisms for intuitive surface modeling. In *4th Eurographics / ACM SIGGRAPH Symposium on Geometry Processing (SGP'06)* (2006), pp. 11–20.

[BPWG07] BOTSCH M., PAULY M., WICKE M., GROSS

© The Eurographics Association and Blackwell Publishing 2007.

M.: Adaptive space deformations based on rigid cells. *Computer Graphics Forum 26*, 3 (2007). Proc. Eurographics 2007.

[BS91] BLOOMENTHAL J., SHOEMAKE K.: Convolution surfaces. In *Proceedings of AMS SIGGRAPH '91* (1991), pp. 251–256.

[BSPG06] BOTSCH M., SUMNER R., PAULY M., GROSS M.: Deformation transfer for detail-preserving surface editing. In *Vision, Modeling & Visualization* (Aachen, Germany, November 2006), pp. 357–364.

[Chu97] CHUNG F. R. K.: *Spectral Graph Theory*. American Mathematical Society, 1997. CBMS, Regional Conference Series in Mathematics, Number 92.

[Dam05] DAMON J. N.: Determining the geometry of boundaries of objects from medial data. *International Journal of Computer Vision 63*, 1 (2005), 45–64.

[Dam07] DAMON J. N.: Global geometry of regions and boundaries via skeletal and medial integrals. *Communications in Analysis and Geometry* (2007).

[Dav04] DAVIS T. A.: UMFPACK - an unsymmetric-pattern multifrontal method with a column pre-ordering strategy. *ACM Transactions on Mathematical Software 30*, 2 (2004), 196–199.

[DQ04] DU H., QIN H.: Medial axis extraction and shape manipulation of solid objects using parabolic PDEs. In *Ninth ACM symposium on Solid Modeling and Applications (SM'04)* (2004), pp. 25–35.

[DS06] DEY T. K., SUN J.: Normal and feature approximations from noisy point clouds. In *FSTTCS 2006: Foundations of Software Technology and Theoretical Computer Science. LNCS 4337* (2006), pp. 21–32.

[FTS06] FUNCK W. V., THEISEL H., SEIDEL H.-P.: Vector-field-based shape deformations. *ACM Transactions on Graphics 25*, 3 (2006), 1118–1125. Proc. ACM SIGGRAPH 2006.

[GK03] GIBLIN P. J., KIMIA B. B.: On the intrinsic reconstruction of shape from its symmetries. *IEEE Trans. Pattern Anal. Mach. Intell. 25*, 7 (2003), 895–911.

[HBK02] HISADA M., BELYAEV A. G., KUNII T. L.: A skeleton-based approach for detection of perceptually salient features on polygonal surfaces. *Computer Graphics Forum 21*, 4 (2002), 1–12.

[HSL*06] HUANG J., SHI X., LIU X., ZHOU K., WEI L., TENG S., BAO H., GUO B., SHUM H.-Y.: Subspace gradient domain mesh deformation. *ACM Transactions on Graphics 25*, 3 (2006), 1126–1134. Proceedings of ACM SIGGRAPH.

[IBP07] ILYA BARAN I., POPOVIĆ J.: Automatic rigging and animation of 3D characters. *ACM Transactions on Graphics 26*, 3 (2007). Proc. ACM SIGGRAPH 2007.

[JMD*07] JOSHI P., MEYER M., DEROSE T., GREEN B., SANOCKI T.: Harmonic coordinates for character articulation. *ACM Transactions on Graphics 26*, 3 (2007). Proc. ACM SIGGRAPH 2007.

[JSW05] JU T., SCHAEFER S., WARREN J.: Mean value coordinates for closed triangular meshes. *ACM Transactions on Graphics 24*, 3 (2005), 561–566. Proc. ACM SIGGRAPH 2005.

[KMP07] KILIAN M., MITRA N. J., POTTMANN H.: Geometric modeling in shape space. *ACM Transactions on Graphics 26*, 3 (2007). Proc. ACM SIGGRAPH 2007.

[KO03] KOBAYASHI K. G., OOTSUBO K.: t-FFD: Free-form deformation by using triangular mesh. In *Eight ACM Symposium on Solid Modeling and Applications* (2003), pp. 226–234.

[LCJ94] LAZARUS F., COQUILLART S., JANCÉNE P.: Axial deformations: an intuitive deformation technique. *Computer-Aided Design 26*, 8 (1994), 607–613.

[LCOGL07] LIPMAN Y., COHEN-OR D., GAL R., LEVIN D.: Volume and shape preservation via moving frame manipulation. *ACM Transactions on Graphics 26*, 1 (January 2007).

[LKA06] LIEN J.-M., KEYSER J., AMATO N. M.: Simultaneous shape decomposition and skeletonization. In *ACM Solid and Physical Modeling Symposium (SPM'06)* (2006), pp. 219–228.

[LMH00] LEE A., MORETON H., HOPPE H.: Displaced subdivision surfaces. In *Proceedings of ACM SIGGRAPH* (2000), pp. 85–94.

[LSCOL05] LIPMAN Y., SORKINE O., COHEN-OR D., LEVIN D.: Linear rotation-invariant coordinates for meshes. *ACM Transactions on Graphics 24*, 3 (2005). Proc. ACM SIGGRAPH 2005.

[MTLT88] MAGNENAT-THALMANN N., LAPERRIÉRE R., THALMANN D.: Joint-dependent local deformations for hand animation and object grasping. In *Graphics Interface '88* (1988), pp. 26–23.

[Nád68] NÁDENÍK Z.: Zur geometrie im grossen der kugelkongruenzen. *Czechoslovak Math. J. 18 (93)* (1968), 700–717.

[PFF*03] PIZER S. M., FLETCHER T., FRIDMAN Y., FRITSCH D. S., GASH A. G., GLOTZER J. M., JOSHI S., THALL A., TRACTON G., YUSHKEVICH P., CHANEY E. L.: Deformable M-reps for 3D medical image segmentation. *International Journal of Computer Vision 55*, 2 (2003), 85–106.

[PP99] PINKALL U., POLTHIER K.: Computing discrete minimal surfaces and their conjugates. *Experimental Mathematics 2*, 1 (1999), 15–36.

[Sie99] SIERSMA D.: Properties of conflict sets in the plane. In *Geometry and Topology of Caustics – Caustics '98* (1999), Banach Center Publ. 50, Polish Acad. Sciences, Warsaw, pp. 267–276.

© The Eurographics Association and Blackwell Publishing 2007.

[Sor06] SORKINE O.: Differential representations for mesh processing. *Computer Graphics Forum 25*, 4 (2006), 789–807.

[SP04] SUMNER R. W., POPOVIĆ J.: Deformation transfer for triangle meshes. *ACM Transactions on Graphics 23*, 3 (2004), 399–405. Proc. ACM SIGGRAPH 2004.

[SPW96] SHERBROOKE C. E., PATRIKALAKIS N. M., WOLTER F.-E.: Differential and topological properties of medial axis transforms. *Graphical Model and Image Processing 58*, 6 (1996), 574–592.

[SSR99] SOTOMAYOR J., SIERSMA D., R. G.: Curvatures of conflict surfaces in Euclidean 3-space. In *Geometry and Topology of Caustics – Caustics '98* (1999), Banach Center Publ. 50, Polish Acad. Sciences, Warsaw, pp. 277–285.

[WSGD00] WOOD Z. J., SCHRÖDER P., GREEN D., DESBRUN M.: Semi-regular mesh extraction from volumes. In *IEEE Visualization 2000* (2000), pp. 275–282.

[WSLG07] WEBER O., SORKINE O., LIPMAN Y., GOTSMAN C.: Context-aware skeletal shape deformation. *Computer Graphics Forum 26*, 3 (2007). Proc. Eurographics 2007.

[YBS03] YOSHIZAWA S., BELYAEV A., SEIDEL H.-P.: Free-form skeleton-driven mesh deformations. In *8th ACM Symposium on Solid Modeling and Applications* (2003), pp. 247–253.

[YHM06] YAN H.-B., HU S.-M., MARTIN R. R.: Skeleton-based shape deformation using simplex transformations. In *24th Computer Graphics Int. Conf. (CGI 2006). LNCS 4035* (2006), pp. 66–77.

[YZX*04] YU Y., ZHOU K., XU D., SHI X., BAO H., GUO B., SHUM H.-Y.: Mesh editing with Poisson-based gradient field manipulation. *ACM Transactions on Graphics 23*, 3 (2004), 641–648. Proc. ACM SIGGRAPH 2004.

[ZHS*05] ZHOU K., HUANG J., SNYDER J., LIU X., BAO H., GUO B., SHUM H.-Y.: Large mesh deformation using the volumetric graph Laplacian. *ACM Transactions on Graphics 24*, 3 (2005), 496–503. Proc. ACM SIGGRAPH 2005.

[ZRKS05] ZAYER R., RÖSSL C., KARNI Z., SEIDEL H.-P.: Harmonic guidance for surface deformation. *Computer Graphics Forum 24*, 3 (2005), 601–609.

Appendix A. Simple geometry of sphere envelopes

Consider a smooth two-parameter family of spheres, a *congruence of spheres*, in 3D. Let the surface of sphere centers be given in a parametric form $\mathbf{s} = \mathbf{s}(u,v)$ and $R = R(u,v)$ be the radius function. Consider an envelope $\mathcal{M}$ of the sphere congruence $[\mathbf{s}, R]$. The envelope allows for a natural parameterization

$$\mathbf{x}(u,v) = \mathbf{s}(u,v) + R(u,v)\mathbf{n}(u,v),$$

where $\mathbf{n}(u,v)$ is the outer (w.r.t the surface of centers) unit normal of the envelope. See Fig. 4 for an illustration. Basis vectors

$$\mathbf{x}_u = \mathbf{s}_u + R_u\mathbf{n} + R\mathbf{n}_u \quad \text{and} \quad \mathbf{x}_v = \mathbf{s}_v + R_v\mathbf{n} + R\mathbf{n}_v \tag{11}$$

are orthogonal to $\mathbf{n}$. Thus, taking the scalar product of (11) and $\mathbf{n}$, we arrive at

$$\mathbf{s}_u \cdot \mathbf{n} = -R_u \quad \text{and} \quad \mathbf{s}_v \cdot \mathbf{n} = -R_v. \tag{12}$$

Denote by $\mathbf{m}$ the orientation normal of the surface of centers $\mathbf{s}(u,v)$. We have

$$\mathbf{n} = \alpha\mathbf{s}_u/|\mathbf{s}_u| + \beta\mathbf{s}_v/|\mathbf{s}_v| + \gamma\mathbf{m} \tag{13}$$

where the direction-cosines α and β are obviously obtained from (12). The remaining direction-cosine γ is easily computed from (13). Thus the direction-cosines of $\mathbf{n}$ depend on the coefficients of the first fundamental form $d\mathbf{s}^2$ of the surface of centers $\mathbf{s}(u,v)$ and first-order derivatives of the radius function $R(u,v)$ along the parametric curves. In particular it means that, for each sphere of the family, the point of contact between the sphere and envelope depends on $d\mathbf{s}^2$ and R_u, R_v only. Further, the area element of the envelope

$$(\mathbf{s}_u + R_u\mathbf{n} + R\mathbf{n}_u) \times (\mathbf{s}_v + R_v\mathbf{n} + R\mathbf{n}_v)$$

also depends on $d\mathbf{s}^2$ and derivatives of $R(u,v)$ along the parametric curves of $\mathbf{s}(u,v)$.

Appendix B. Curvature of the skeleton in 2D

Let $\mathcal{C}$ be a closed curve oriented by its outer unit normal $\mathbf{n}$ and $\mathcal{S}$ be the skeleton (medial axis) of the figure bounded by $\mathcal{C}$. Consider the negative offsets of $\mathcal{C}$: $\mathcal{C}_\lambda = \mathcal{C} - \lambda\mathbf{n}$. It is well-known that skeleton $\mathcal{S}$ is generated by the first self-intersections of $\mathcal{C}_\lambda$. Consider a non-singular point $\mathbf{p} \in \mathcal{S}$ generated as a self-intersection of $\mathcal{C}_\lambda$ for a certain value of offset parameter λ and denote by φ the angle between one of the tangents of $\mathcal{C}_\lambda$ and the tangent of $\mathcal{S}$ at $\mathbf{p}$. Direct computations [Sie99] show that the curvature κ of $\mathcal{S}$ at $\mathbf{p}$ is given by

$$\kappa = \frac{1}{2}\left(\frac{k_1}{1-\lambda k_1} - \frac{k_2}{1-\lambda k_2}\right)\cos\varphi, \tag{14}$$

where k_1 and k_2 are the curvatures of $\mathcal{C}$ computed at the points $\mathbf{q}_1$ and $\mathbf{q}_2$ corresponding to $\mathbf{p}$, respectively. Equation (14) implies that

$$2\kappa d\mathbf{s} = k_1\, d\mathbf{s}_1 - k_2\, d\mathbf{s}_2, \tag{15}$$

where $d\mathbf{s}_1$ and $d\mathbf{s}_2$ are the oriented length elements of $\mathcal{C}$ at $\mathbf{q}_1$ and $\mathbf{q}_2$, respectively, and $d\mathbf{s}$ is the oriented length element of $\mathcal{S}$ at $\mathbf{p}$.

Denote by $\mathcal{S}'$ a set of smooth curve segments obtained from the double skeleton $\tilde{\mathcal{S}}$ by removing its singular points. From (15) it follows that

$$\int_{\mathcal{S}'} |\kappa|\, ds \le \int_{\mathcal{C}} |k|\, ds$$

which means that $\mathcal{S}'$ is less curved than $\mathcal{C}$.

© The Eurographics Association and Blackwell Publishing 2007.